

On the origin of ultra high energy cosmic rays: Subluminal and superluminal relativistic shocks

Athina Meli^{a,b,*}, Julia K. Becker^{b,c,*}, John J. Quenby^d

^a*Department of Physics, National University of Athens, Panepistimiopolis
Zografos 15783, Greece*

^b*Institut für Physik, Universität Dortmund, 44221 Dortmund, Germany*

^c*Institutionen för Fysik, Göteborgs Universitet, 41296 Göteborg, Sweden*

^d*High Energy Physics Group, Blackett Laboratory, Imperial College London,
Prince Consort Road SW7 2BZ, UK*

Abstract

The flux of ultra high energy cosmic rays (UHECRs) at $E > 10^{18.5}$ eV is believed to arise in plasma shock environments in extragalactic sources. In this paper, we present a systematic study of particle acceleration by relativistic shocks, in particular concerning the dependence on bulk Lorentz factor and the angle between the magnetic field and the shock flow. For the first time, simulation results of super- and subluminal shocks with boost factors up to $\Gamma = 1000$ are investigated and compared systematically. While superluminal shocks are shown to be inefficient at the highest energies ($E > 10^{18.5}$ eV), subluminal shocks may provide particles up to 10^{21} eV, limited only by the Hillas-criterion. For the subluminal case, we find that mildly-relativistic shocks, thought to occur in jets of Active Galactic Nuclei (AGN, $\Gamma \sim 10 - 30$) yield energy spectra of $dN/dE \sim E^{-2}$. Highly-relativistic shocks expected in Gamma Ray Bursts (GRBs, $100 < \Gamma < 1000$), on the other hand, have spectra as flat as $E^{-1.5}$. The model results are compared to the measured flux of cosmic rays (CRs) at the highest energies and it is shown that, while AGN spectra are well-suited, GRB spectra are too flat to explain the observed flux. The first evidence of a correlation between the cosmic ray flux above $5.7 \cdot 10^{10}$ GeV and the distribution of AGN by Auger are explained by the model. Neutrino production is expected in GRBs, either in mildly or highly relativistic shocks and although these sources are excluded as the principle origin of UHECRs, superluminal shocks in particular may be observable via neutrino and photon fluxes, rather than as protons.

Key words: relativistic shocks, acceleration, AGN, GRBs, cosmic ray spectrum, cosmic ray origin, cosmic neutrinos

PACS: 52.35.Tc, 52.38.Ph, 95.85.Ry

* Corresponding authors:

ameli@phys.uoa.gr, phone: +30-210-727-6908

julia.becker@physics.gu.se, phone: +46-31-7723190

1 Introduction

The observation of the energy spectrum of ultra high energy cosmic rays (UHE-CRs) indicates the presence of an extragalactic component at $E > 10^{18.5}$ eV. Active Galactic Nuclei (AGN) and Gamma Ray Bursts (GRBs) seem to be the two most promising source candidates for the production of charged cosmic rays (CRs). Work in the late 1970s by a number of authors, e.g. Krymskii (1977); Bell (1978a,b), who based their idea on the original Fermi acceleration mechanism, first presented by Fermi (1949, 1954), established the basic mechanism of particle diffusive acceleration in non-relativistic shocks. In this mechanism, individual particles are accelerated in a collisionless magnetised plasma by scattering off magnetic irregularities to recross a shock front many times. Since then, considerable analytical and numerical investigations have been performed, but more questions need to be answered concerning the acceleration mechanism at relativistic shock speeds.

In this work, we will present a series of simulation studies varying the shock velocity and the magnetic field inclination to the shock normal, applying various particle scattering media, fixed in the plasma flow frame, aiming to provide a more refined determination of the possible spectra which could result. All shocks under investigation are taken to be oblique, so that the magnetic field is neither aligned with nor strictly perpendicular to the shock front normal. Parallel shock simulation studies were given in Meli and Quenby (2003a). Monte Carlo calculations will be performed in the relativistic shock environments believed to occur in AGN and GRB jets. The resulting very high energy CR spectra and the subsequent multiwavelength radiation observation from candidate sources, such as AGN and GRBs, will be mentioned.

Previous work by Meli and Quenby (2003a,b), on simulation studies for subluminal and superluminal shocks did not establish the relationship between spectral slope, shock inclination angles, shock velocity and particle scattering model which will be considered here. These past studies amongst others investigated the 'traditional' large angle scattering model and the pitch angle diffusion model of particles, but only for the extreme limiting case of $\delta\theta \leq 1/\Gamma$. In the present work we will allow for pitch angle scattering to vary between $1/\Gamma \leq \delta\theta \leq 10/\Gamma$ to correspond to a variety of scattering wave models. We will establish the spectral index dependence on the Γ of the shock. The shock obliquity will be varied while using a series of high velocity plasma flows, ranging from $\Gamma = 10 - 1000$. The contribution of the high energy CRs from AGN and GRBs to the observed diffuse CR spectrum will be discussed, based upon the simulated spectra.

In Section 2, details of the simulation are discussed. Section 3 presents the resulting spectra emphasising the spectral dependence on the relativistic flow

Lorentz factor. The calculated spectra are used to estimate a possible contribution of AGN and GRBs to the observed diffuse spectrum of charged CRs. The implications for high energy neutrino and photon emission is discussed in Section 4. Finally, in Section 5 the results are summarised.

1.1 Source Candidates for relativistic shocks

The energy budget available for UHECRs production in GRBs is approximately 2×10^{44} erg/Mpc³/yr, as concluded from the observed gamma-ray GRB release rate. This energy budget corresponds to the required energy release rate of $> 10^{18.5}$ eV of UHECRs and is based on an assumed star formation rate (SFR) history (Vietri, 1995; Waxman, 2000) with about 1 burst/Gpc³/yr at $z = 0$. The typical luminosity of AGN, $L \sim 10^{42} - 10^{47}$ erg/s is also sufficient to explain the UHECR flux under the assumption that AGN follow the SFR. For example, Moran et al. (2001) find an average luminosity from an estimated 95 X-ray active AGN within 60 Mpc of 4.8×10^{44} erg/s, this distance being the cosmic ray absorption horizon at about 2×10^{20} eV. Within the regions of local space accessible to cosmic ray diffusion, the energy supply over a Hubble time is 6.6×10^{-16} erg/cm³. By comparison the GRB supply is 6.7×10^{-20} erg/cm³. With GRBs as the most luminous transient objects in the sky and AGN as the most luminous permanent ones, these two source classes are the best candidates for the acceleration of UHECRs, following the arguments of Hillas (1984).

The observation of electron synchrotron radiation in the radio regime indicates that mildly-relativistic shocks of boost factors $\Gamma \approx 10 - 30$ are present in the jets of AGN (Biermann and Strittmatter, 1987; Falcke et al., 1995). The photon spectrum of AGN is broadband, ranging from radio up to TeV emission in the case of optically thin sources. Assuming that hadrons are accelerated along with the electrons in the jet, AGN are good candidates to be responsible for at least a significant fraction of the extragalactic component of the CR flux.

The observation of the highly variable, prompt GRB photon spectra at soft photon energies ($E_\gamma > 100$ keV) indicate the acceleration of electrons in highly relativistic shocks of boost factors around $100 < \Gamma < 1000$, see Halzen and Hooper (2002) and references therein. However, mildly relativistic internal shocks may also occur within the GRB plasma flow. Protons are believed to be accelerated up to $\sim 10^{21}$ eV as discussed by Waxman (2000). The total release of electromagnetic energy by GRBs has led to the suggestion that the CR spectrum above the ankle ($E > 10^{18.5}$ eV) can be explained by GRBs (Vietri, 1995).

1.2 Maximum energy

A basic physical limitation to the maximum energy of the accelerated particles is the size of the acceleration region and the magnetic field present. Parker (1958a,b,c, 1966) first discussed this CR energy limitation within the solar system. Later on Hillas (1984) extended the CR energy limit argument to a number of astrophysical sources. Particles must escape once the gyration radius exceeds the source radius. The maximum energy is then given as

$$E_{\max}^{18} = \beta_s \cdot Z \cdot B_{\mu G} \cdot L_{kpc}. \quad (1)$$

Here, $E_{\max}^{18} := E_{\max}/(10^{18} \text{ eV})$ is the maximum energy that can be achieved, $\beta_s = V_s/c$ and is equal to 1 for the oblique shock conditions (Jokipii, 1987), Z is the charge of the accelerated particle in units of the charge of the electron, e . Furthermore, $B_{\mu G} := B/(1 \mu\text{G})$ is the magnetic field of the acceleration region in units of $1 \mu\text{G}$ and $L_{kpc} := L/(1 \text{ kpc})$ is the size of the acceleration region in units of 1 kpc . As discussed by Hillas (1984), AGN cores, radio galaxy lobes, and hot spots, are promising candidates for the acceleration of the highest energy events. A second criterion of Hillas that the proton synchrotron loss time should not be less than the acceleration time, is easily met by proton shock acceleration if the shock is relativistic since the acceleration time is

$$\tau_{acc} = \frac{3 \times 10^3 X E_{18}}{B_{\mu G}} \text{ year}, \quad (2)$$

where the scattering mean free path is X times the Larmor radius and the synchrotron loss time is

$$\tau_{synch} = \frac{1.4 \times 10^{14}}{E_{18} B_{\mu G}^2} \text{ year}. \quad (3)$$

As mentioned before, boost factors in AGN are typically assumed to be around $\Gamma \sim 10$, although in special cases, the boost factor can reach up to $\Gamma \sim 30-40$. It is, however, possible that the shock itself happens within a general relativistic environment (Biermann and Strittmatter, 1987) and so the shock is not necessarily relativistic. Here, we assume relativistic movement of the shock front. The magnetic field can be up to $B \sim 10^{-3} \text{ G}$ in the jet at a radius of $r \sim 1 \text{ kpc}$ and the field typically decreases inversely with the radius. This condition allows for particle acceleration up to the highest energies, i.e. $E_{\max}^{AGN} \sim 10^{21} \text{ eV}$ (Biermann and Strittmatter, 1987). Radio galaxy hot spots allow for acceleration of particles up to 10^{21} eV and energies of 10^{19} eV can be produced in radio galaxy lobes. Other suggested sources are not able

to produce particles of sufficient energy because the field strengths available are insufficient to contain the particles.

GRBs may also accelerate protons to 5×10^{20} eV. This is because fields up to $\Gamma B = 10^{14}$ G can be produced at an accretion torus at about 6×10^6 cm radius in massive star collapse before quantum mechanical dissipation, limits the field amplification (Lerche and Schramm, 1977) and the subsequent $1/r$ field fall-off yields an E_{\max} independent of r . Acceleration occurs without significant synchrotron losses, see Vietri (1995); Waxman (2000). The acceleration of particles during the prompt emission phase in highly-relativistic shocks ($\Gamma = 100 - 1000$) is discussed in the following. Acceleration in external shocks during the slowing afterglow phase is also possible so that the spectra may resemble the AGN spectra that we calculate and present in Section 3.

2 The physical concept and the Monte Carlo simulations

Begelman and Kirk (1990) have claimed that most upstream field configurations at high shock boost factors Γ appear *superluminal*. In superluminal shocks the particles are accelerated in a shock drift because there is no transformation into a de Hoffmann-Teller (HT) frame (de Hoffmann and Teller, 1950), where $\vec{E} = \vec{0}$. To transform from the normal shock frame (NSH) to the HT frame, we need to boost by a speed V_{HT} along the shock frame, where $V_{HT} = V_{NSH} \cdot \tan \psi$ (ψ is the angle between the magnetic field and the shock normal). Due to physical causality, this transformation is only possible if V_{HT} is less or equal to the speed of light. Thus, when $V_{NSH} = c$, the limit is $\tan \psi = 1$. When $\tan \psi \leq 1$ the *subluminal* shock transformation case is applied. For all other cases, where a HT frame cannot be found due to a very high inclination in combination with a high shock velocity, the superluminal shock condition applies. While in the subluminal case particle transmission at the shock can be decided in the HT frame employing conservation of the first adiabatic invariant, in the superluminal case computations are followed entirely in the fluid rest frames with reference to the shock frame simply employed to check whether upstream or downstream shock conditions apply.

Superluminal shock acceleration may be treated as a shock drift mechanism in the shock frame and is best visualised when the shock is nearly perpendicular. As viewed in the shock rest frame, the particle is moving in a steep magnetic field gradient perpendicular to the shock surface. The plasma motion at an angle to the magnetic field creates an electric field given by $\vec{E} = -\vec{u} \times \vec{B}/c$. In this mechanism, scattering is unimportant and particles can be accelerated by just one shock encounter. However, due to the high field inclination, a particle gyrating around the field lines crosses the shock more than once in one shock encounter and thus obtains significant additional energy. The drift

is in a direction perpendicular to the magnetic field gradient (shock normal) and the magnetic field, according to

$$\vec{V}_d = \frac{p \cdot c \cdot u}{3e} \left(\frac{\vec{B} \times \nabla B}{B^2} \right), \quad (4)$$

with $B = |\vec{B}|$. The drift direction is such as to cause the particle's energy to increase.

Meli and Quenby (2003a,b) showed that a transformation from an initially isotropic rest frame distribution to an accelerated flow frame leads to a co-moving relativistic plasma frame field distribution lying close to the flow vector. This condition allows for a range of subluminal situations when viewed in the shock frame. Begelman and Kirk (1990) pointed out, on the other hand, that in the blast wave frame the turbulence can be isotropic and many shock stationary frame configurations can be superluminal. In general, flow into and out of the shock discontinuity is not along the shock normal, but a transformation is possible into the NSH frame to render the flows along the normal (Begelman and Kirk, 1990). We assume that such a transformation has already been made.

Vietri et al. (2003) raise the question as to the correct reference frame in which jet acceleration should be viewed. To become CRs, the protons escape sideways out of the narrow beamed jet and are seen in the extragalactic rest frame. Escape upstream into the ambient medium is very unlikely. Strictly speaking, we need to employ a transformation conserving the distribution function f depending on the momentum p , so $f(p) = f'(p')$ (Forman (1970) demonstrates this invariance which is related to Liouville's theorem). Here, $p^2 f(p) = dJ(E(p), \vec{n})/dE$, where $f(p)$ is in the direction of vector \vec{n} and the energy E corresponds to the momentum vector \vec{p} . The particle flux dJ/dE is typically in units of $\text{cm}^{-2} \text{ s}^{-1} \text{ sr}^{-1} \text{ GeV}^{-1}$. Prime and unprimed denote rest frame and observer's frame. For our calculations we choose the total energy normalisation to be done in the shock frame. While the transformation affects the maximum energy obtained in the rest frame to some extent, the fact that escape from the beamed jet is mainly by motion perpendicular to the flow, means that we are chiefly involved in transforming a momentum vector perpendicular to the relative velocity of the reference frames, where there is no Lorentz correction. For X-ray production in shocks the relevant results are in the downstream frame.

The purpose of the Monte Carlo simulations is to find a solution to the particle transport equation for highly-relativistic flow velocities. The appropriate time

independent Boltzmann equation is given by the following

$$\Gamma(V + v\mu)\frac{\partial f}{\partial x} = \frac{\partial f}{\partial t}|_c, \quad (5)$$

where a steady state is assumed at the shock rest frame, and V is the fluid velocity, v the velocity of the particle, Γ the Lorentz factor of the fluid frame, $\mu = \cos\theta$ the cosine of the particle's pitch angle θ and $\partial f/\partial t|_c$ the collision operator.

Particle scattering by magnetic irregularities fixed in the plasma frame will be assumed. The Alfvén velocity, V_A , for AGN jets with a maximum 10^{-3} G field and a particle density of 10^{-2} cm $^{-3}$ is 2×10^9 cm/s. For GRB jets with a 10 G field and a particle density of 10^6 cm $^{-3}$, it is of similar magnitude. With these wave velocities, the waves will appear almost stationary to relativistic particles and second order Fermi acceleration, with a fractional energy gain $(V_A/c)^2$, is small compared with shock acceleration where a single encounter cause energy enhancement by a Γ^2 factor. $V_A \rightarrow c/\sqrt{3}$ is the theoretical relativistic limit to wave speed and to shock speed in the fluid frame while numerical jet simulation suggests large scale, knot features travel at about $c/10$ (van Putten, 2005). Thus, we seem justified in neglecting fluid frame acceleration beyond the region of trajectory intersection with the shock surface. This is especially true downstream where the second order Fermi fractional gain per collision is limited to $1/12$.

The scattering operator will be treated via a pitch angle scattering approach, rather than as previously in the work of Meli and Quenby (2003a,b) where large angle scattering was considered. In standard kinetic theory the spatial diffusion coefficients κ_{\parallel} and κ_{\perp} , are related to the formula $\kappa_{\perp} = \kappa_{\parallel} \cdot (1 + (\lambda/r_l)^2)^{-1}$, Jokipii (1987). In the well known Bohm Limit, $\lambda/r_l = 1$, but interplanetary particle propagation studies and gyroresonance theory suggest λ to be a number of particle gyroradii r_l , that is $\lambda \geq 10r_l$. Hence, in the shock normal, or in the x direction, the diffusion coefficient is given by $\kappa_{\parallel} = \lambda v/3$ where $\kappa = \kappa_{\parallel} \cos^2\psi$, since we assume that $\kappa_{\parallel} \gg \kappa_{\perp}$. A guiding centre approximation is therefore used to follow propagation along field lines. Because relativistic shocks generate strong small-scale turbulent magnetic field downstream by the relativistic two stream instability (Medvedev, 1999), we assume power in the scattering increases, as does the field strength and for simplicity we assume these quantities change to keep their ratio constant. Therefore, $\lambda_{down} = \lambda_{up}$.

Gallant et al. (1999) have demonstrated analytically that particles entering the upstream region in a direction nearly normal to the shock can only experience small-angle scattering (pitch angle diffusion), $\delta\theta \leq 1/\Gamma$ with $\delta\theta$ measured in the upstream fluid frame for scattering in a uniform field or a randomly

oriented set of uniform field cells. The condition arises because particles attempting to penetrate upstream from the shock are swept back into the shock before they can scatter far from it. If we consider the ratio of initial energy to final energy, measured in the upstream or 'primed' frame, after up to down to up transmission in an inclined shock, we have

$$E'_f/E'_i = \Gamma^2(1 + \beta_r \mu'_{\rightarrow d})(1 - \beta_r \mu^*_{\rightarrow u}) \quad (6)$$

where β_r is the relative velocity of the frames as a fraction of c , $\mu'_{\rightarrow d}$ is the cosine of the particle velocity angle to the normal direction in the upstream frame at the moment of going downstream and $\mu^*_{\rightarrow u}$ is cosine of the particle velocity angle to the normal in the downstream frame at the moment of going upstream. For down to up crossing, $-\mu^*_{\rightarrow u} > B_1^t/B_2^t$ where B_1^t/B_2^t is the inverse compression ratio. Up to down, the pitch angle scattering constraint is $\mu'_{\rightarrow d} \approx -1 + 1/\Gamma^2$. As pointed out by Baring (1999), $E'_f/E'_i \approx 2$. On the first up to down to up cycle with injection upstream and directed towards the shock, $E'_f/E'_i \approx \Gamma^2$, corresponding to the large angle scattering case of Quenby and Lieu (1989). Since this constraint is largely dependent on the kinematic competition between upstream particle flow and the relativistic approach of the shock front, it is not critically dependent on the exact magnitude of the pitch angle scattering. Moreover, as shown by Quenby and Meli (2005), blobs of high field scattering centres which could cause even large angle scattering, are allowed if the Larmor radius in the blob, $r_{g,b}$, satisfies $(\lambda/2\Gamma^2) > r_{g,b}$ where the parallel mean free path $\lambda = X r_{g,ambient}$ and $X \sim 10$. Such fields would allow for substantial scattering before particles are swept back to the shock. This criterion, derived for parallel shocks, effectively applies in the oblique, subluminal case since in the upstream frame, the field direction is near the normal direction. To obtain a deflection $\sim 10\Gamma^{-1}$, the constraint is relaxed to $b/B > \approx 2\Gamma$ as the ratio of 'blob' to ambient field, where b is the perpendicular perturbation to the mean field, B . Hence, a relatively few field blobs, perhaps originating in strong instability in a hypernova collapse and with field strengths up to a factor 1000 stronger than the ambient, would thus be required to allow for pitch angle scattering greater than $\delta\theta = 1/\Gamma$. For practical purposes, remembering it is the downstream scattering that is relevant to particle loss, it seems reasonable to use larger values of $\delta\theta$, within the pitch angle diffusion model.

A simple representation for the effect of the turbulence which relates to previous work is to suppose the particle scatters $\delta\theta = N/\Gamma$ every $\lambda = 10r_l$ where r_l is the Larmor radius, in the plane of gyration. A transverse field perturbation changes the pitch angle in a quasi-linear theory (Kennel and Petscheck, 1966), by

$$\delta\theta = \omega \frac{b}{B} \delta t \quad (7)$$

in a time δt due to a perpendicular perturbation, b , to the mean field, B , with cyclotron angular frequency, $\omega = eB/\gamma m_o c$. The particle moves in near gyroresonance with the wave in b . A pitch angle diffusion coefficient can then be derived

$$D_\theta = \frac{\delta\theta^2}{\delta t} = \frac{\omega^2}{v_\parallel} \frac{P(k)}{B^2}, \quad (8)$$

where $P(k) = P_o k^s$ is the power spectral density of b at gyroresonance wave number $k = \omega/v_\parallel$. A particle then diffuses in pitch by a finite amount, $\delta\theta$ during δt given by

$$\delta\theta^2 = 2D_\theta \delta t. \quad (9)$$

It is waves, of wave number k , fulfilling the gyroresonance condition, $k = \omega/v_\parallel$ that cause the scattering of particles satisfying $\omega r_l = v_\perp$. We choose $\delta\theta$ to lie between $1/\Gamma$ and $10/\Gamma$, so on average a particle scatters $5/\Gamma$ after a time $10\sqrt{3}r_l/c$ so that

$$\delta\theta^2 = \frac{25}{\Gamma^2} = \frac{2\omega^2}{v_\parallel B^2} P_o(k) \frac{\omega^s}{v_\parallel^s} \frac{10\sqrt{3}v_\perp}{c\omega}. \quad (10)$$

To choose $\delta\theta$ independent of particle γ that is of ω , we require $s=-1$ for the spectral slope. Then we obtain a power spectrum relative to the mean field power

$$\frac{P(k)}{B^2} = \frac{5}{4\sqrt{2}\Gamma^2} k^{-1}. \quad (11)$$

The total fractional power in the turbulence if resonating waves are present to scatter particles of between $\gamma = 300$ and $\gamma = 10^{12}$ is $1.4/\Gamma^2$. Hence, the chosen pitch angle scattering model corresponds to a weak turbulence situation. Because quasi-linear theory for wave particle interactions is known to be an inexact approximation, the power spectrum we have presented must also be an approximation to the scattering model we employ. The choice of a fixed factor, 10, in the relation between λ and r_l acknowledges this inexactness. The spectrum is simply presented to provide a link with the work of others, especially Niemec and Ostrowski (2005) who realise the field fluctuations employing a specified wave spectrum. In the present investigation, we allow the particles with pitch angle chosen at random to lie in the range of $1/\Gamma \leq \delta\theta \leq 10/\Gamma$. In our past work mentioned in Section 1, we presented results for the large angle case and the aforementioned extreme limiting case of $\delta\theta \leq 1/\Gamma$.

Our past studies of pitch angle scattering Meli and Quenby (2003a,b) suggested that as the magnetic field inclination angle to the shock normal decreased, the spectra become smoother. Both a pronounced, plateau-like structure and increasing flatness developed for the highest values of the shock boost factor Γ . Additionally, for all inclination values used in the simulations, for $\Gamma = 10 - 30$, the spectral form remains smooth. Ellison and Double (2004), Stecker et al. (2007) and references therein, have shown similar trends. In this more comprehensive study, the previous claims will be more thoroughly investigated.

Standard theory poses the conservation of the first adiabatic invariant in the HT frame in order to determine reflection or transmission of the particles. Since in this frame the allowed and forbidden angles for transmission depend only on the input pitch and phase, not on rigidity, the results of Hudson (1965) apply in our model. For an isotropic flux, the transmission coefficient ζ is simply given by the particle flux conservation between an upstream magnetic flux tube area and the corresponding downstream flux tube area to which it connects

$$\zeta = \frac{FB_1}{FB_2}, \quad (12)$$

where F is the distribution function (Parker, 1965). Trajectory integration, Hudson (1965) giving the phase dependence of the probability of transmission as a function of phase and pitch angle showed that the reflection percent plotted against pitch angle never varied more than 20% from the mean value and these results were consistent with the flux conservation prediction based on Parker (1965) and the adiabatic invariant conservation. In the relativistic shock situation anisotropy renders the input to the shock from upstream, very anisotropic in pitch angle, but as was discussed in Meli (2003), it is an acceptable approximation to randomise phase before transforming to the HT frame and then to use the adiabatic invariant to decide on reflection/transmission, because of the Hudson result.

For further details on the simulations, see appendix A.

3 Results

The physical concepts and analytical approximations previously mentioned are used to perform Monte Carlo simulations for relativistic superluminal and subluminal shocks. Computed particle spectra will be presented with special focus on the relation between a given astrophysical source shock boost factor Γ and the resulting spectral features. Of particular relevance is Section 3.2

devoted to the calculation of the contribution of these sources to the observed diffuse CR spectrum.

3.1 CR shock acceleration spectra

3.1.1 Superluminal shock spectra

Initially, we present simulations for relativistic superluminal shocks as described in the previous section and the Appendix. Unlike our previous work which was confined to large angle scattering, pitch angle scatter is employed. The guiding centre approximation is used except within one complete particle helical cycle from the shock. Since a transformation into the HT frame is not possible as described in Section 2, the particles are followed in the appropriate fluid rest and SH frames, simulating the physical picture of the shock drift mechanism. We follow the helix trajectory of the particle until it intersects with the shock front, applying a pitch angle scatter [$\delta\theta \leq 10/\Gamma, \phi \in (0, 2\pi)$] right up to the shock interface. Simulation runs performed showed that the results were basically independent of ψ , magnetic field to shock normal angle. We therefore show here a simulation run with an arbitrarily chosen inclination angle, $\psi = 76^\circ$, as an example, employing a range of boost factors. The resulting spectra are presented in the shock frame on the downstream side as we want to ensure comparability with following calculations.

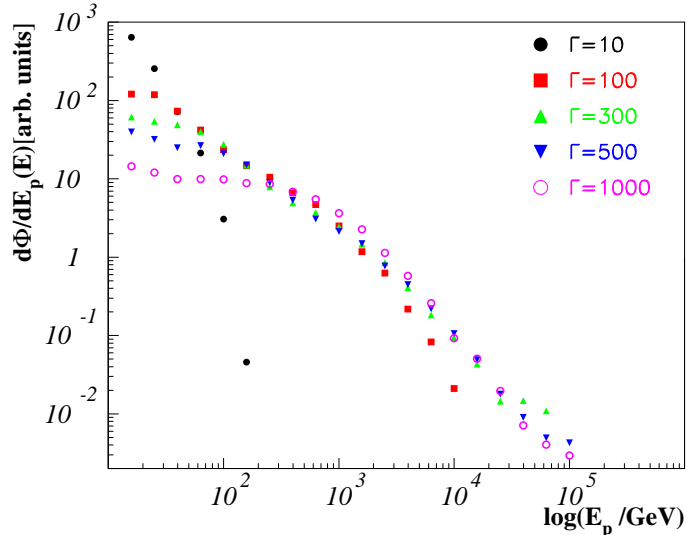


Fig. 1. Superluminal, relativistic spectra at $\psi = 76^\circ$. Boost factors are varied between $\Gamma = 10, 100, 300, 500, 1000$. Spectra for different inclination angles ψ are comparable.

The resulting particle spectra for $\Gamma = 10, 100, 300, 500$ and 1000 are displayed

in Fig. 1. These plots indicate that for mildly-relativistic shocks ($\Gamma = 10$), the acceleration is efficient up to energies $E_p < 10^2$ GeV. More highly-relativistic shocks ($\Gamma \geq 100$) can produce particles up to $E_p < 10^5$ GeV. The upper limit of significant acceleration is $\sim \Gamma^2$, corresponding to only one complete particle crossing cycle with the majority of particles either failing to return a second time or only returning at angles close to the normal. In the region of efficient acceleration, the spectra approximately follow power-laws with spectral indices lying between $\sim 2.0 - 2.3$. In contrast, for the case of large angle scattering, previously studied by Meli and Quenby (2003b), the spectra could not be described by power-laws, but exhibited a concave shape terminating in a steep energy cut-off.

We conclude that superluminal, relativistic shocks are not efficient accelerators for very high energy particles and are unlikely to contribute to observable effects, discussed in more detail in Section 3.2. These conclusions concur with the work of Niemec and Ostrowski (2007). While superluminal shocks cannot contribute to the observed spectrum of charged UHECRs, a contribution to the neutrino- and TeV-photon background arising from proton-photon or proton-proton interactions, is still possible as discussed in Section 4.

3.1.2 Subluminal shock spectra

Particle spectra produced in relativistic subluminal shocks have been calculated for three different inclination angles in the shock frame, $\psi = 23^\circ$, 33° and 43° which we chose as representing the possible range of subluminal shock angles likely in astrophysical sources. In appendix B, simulated particle spectra are presented for the entire energy range of particle energy considered, $E = 10^2 - 10^{12}$ GeV, for a range of boost factors, $\Gamma = 10$ to $\Gamma = 1000$ and for all three angles. The chief result is that the spectra appear as smooth power-laws for mildly-relativistic shocks, $\Gamma \leq 30$. As the boost factor increases, the spectra appear with bumps ($\Gamma > 100$): The plateau-like parts of the spectra at higher energies and higher boost factors are caused by particles continuing to undergo significant acceleration in a second cycle. The lower energy part of the spectrum is dominated by particles undergoing one acceleration shock crossing while the second bump in the spectrum represents particles experiencing two acceleration shock crossings. In this first complete shock cycle crossing from upstream to downstream to upstream, the energy gain is a factor Γ^2 , operating an injection energy already $\approx \Gamma$ in magnitude. Subsequent crossings become smoother since the energy gain is expected to be limited to ~ 2 and there is a statistical smoothing of the energy gains. At the highest boost factors we investigate, this smoothing regime is not reached.

In order to get a representative picture, we average the particle spectra over the three angles at a particular Γ , in all following calculations. This should

give a more realistic view of the diffuse particle flux from extragalactic sources, as it is expected that a range of angles is likely to occur in the class of AGN and GRB shocks. We concentrate on the highest energies because observation of particle-induced air showers at energies between $10^{9.5}$ GeV and $10^{10.5}$ GeV indicates an extragalactic origin of the charged CRs, distinct from a dominant, galaxy produced component at lower energies. A power-law fit is made to the simulated spectra between $10^{9.5}$ GeV and $10^{10.5}$ GeV. Figure 2 shows the averaged, simulated spectra between $10^{8.5}$ GeV and 10^{11} GeV. At even higher energies, the spectrum is altered by the absorption of protons due to interactions with the cosmic microwave background. While the normalisation of the spectra is arbitrary since dependent on the number of injected particles in the Monte-Carlo simulation, the spectral index can be compared to what is observed in CRs in the same energy range. Table 1 shows the variation of the spectral index with the boost factor. While mildly-relativistic shocks show indices around $\alpha_p \approx 2$, highly-relativistic shocks with $\Gamma > 100$ have flatter spectra between $0.7 < \alpha_p < 1.5$. Particle spectra emitted during the prompt phase of GRBs ($\Gamma > 100$) will therefore appear much flatter than AGN particle spectra ($\Gamma \sim 10$). This has important implications for the interpretation of the origin of the UHECR spectrum as will be discussed in a following subsection.

Stecker et al. (2007) investigating parallel shocks up to $\Gamma = 30$ found increasing spectral structure and decreasing slope as Γ increased ($E^{-1.26}$ at $\Gamma = 30$), trends we have shown to extend to far higher Γ factors and for a more general class of subluminal shock inclination angles. Bednarz and Ostrowski (1998) used pitch angle scattering and varying cross-field diffusion and found that at low Γ , steep spectra occurred at large inclination angles but all values of these parameters seemed to produce spectral slopes of -2.2 at $\Gamma = 243$. In contrast, Meli and Quenby (2003a) found spectra flatter than E^{-1} for parallel shocks as $\Gamma \rightarrow 1000$. Later work, however, with wave spectra $P(k) \sim k^{-1 \rightarrow 1.5}$ by Niemec and Ostrowski (2005) found spectra flatter than E^{-1} with noticeable structure spectra in inclined, subluminal shocks at upstream velocities of $0.5c$. Their trajectory integrations took into account cross field diffusion. Baring (2004) however, cites previous work with no cross field diffusion which finds significant relativistic, inclined shock acceleration to be limited to inclination angles $\leq 25^\circ$. It is not clear whether the very steep spectra quoted at higher inclination angles are due to the steep slope at the edge of the first plateau we mention above, or whether there is a significant difference from our modelling. A high perpendicular diffusion coefficient, high inclination shock situation might be expected to approach a high scattering, parallel shock regime, but this possibility does not seem to reconcile the various conflicting results just discussed. There is an agreement that at very high inclinations significant acceleration above that due to a single shock cycle is ruled out. Also, there seems to be a developing consensus that high Γ , subluminal shocks result in flatter spectra than E^{-2} . Dingus (1995) provides gamma-ray burst evidence for relativistic electron spectra with relatively flat slopes with exponents at

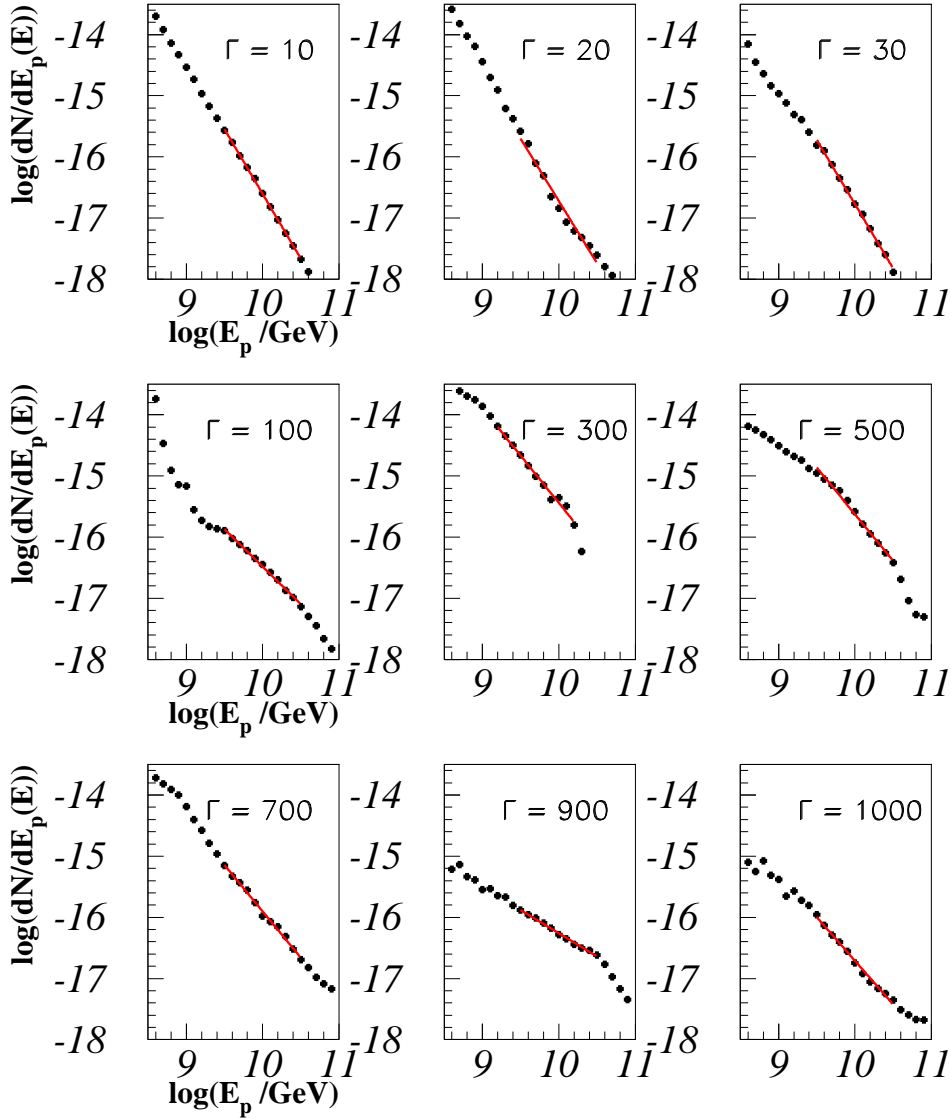


Fig. 2. Subluminal spectra averaged over the three angles for different Γ : $\Gamma = 10, 20, 30$ is displayed in the first row, in the middle, $\Gamma = 100, 300, 500$ is shown and $\Gamma = 700, 900, 1000$ is the bottom row. The black crosses in each graph represent the simulation result. The straight line shows the single power-law for comparison.

least as low as ≈ -2 .

Results indicating a variety of possible slopes are also consistent with radio data on the electron spectra injected at terminal hotspots in the lobes of powerful FR-II radio galaxies where no single, universal power-law is found, as shown by Rudnick et al. (1994) and Machalski et al. (2007) among others.

Γ	10	20	30	100	300	500	700	900	1000
α_p	2.1	2.0	2.1	1.2	1.5	1.5	1.5	0.7	1.4

Table 1

Spectral indices for a single power-law comparison for subluminal shocks. The spectral fits were made between $10^{9.5}$ GeV and $10^{10.5}$ GeV in order to be comparable to the observed CR flux at the same energies. The uncertainty from the fit is less than 10% if we assume an accuracy of the simulation is better than $\Delta \log(dN/dE_p) \sim 0.5$, which is a conservative estimate.

3.2 Diffuse CR spectra from GRBs and AGN

The source spectra derived previously can be translated into an expected diffuse proton flux from astrophysical sources by folding the spectra with the spatial distribution of the sources. In this section, AGN and GRBs are used as potential candidates because these are the sources with the highest observed output in relativistic electrons. Since the particle spectra are strongly dependent on Γ , it is important to discuss which spectra to use for these two source classes. Spectral choice is investigated in the next subsection before the actual calculation of the diffuse spectra is shown. In the last subsection, the results of our calculations are compared to CR data.

3.2.1 AGN and GRBs - intrinsic spectra

Spectral fits limited to the energy range $10^{9.5}$ GeV to $10^{10.5}$ GeV of extragalactic origin are employed for both AGN and GRB sources, but the boost factors applicable differ between these source classes.

The boost factor deduced from electron synchrotron observation can vary significantly in the case of GRBs. While the majority of sources are estimated to have boost factors around $\Gamma \approx 300$, more moderate values down to $\Gamma = 100$ or more extreme values up to $\Gamma = 1000$ are believed to occur. However, the exact distribution of Gamma Ray Burst Γ factors cannot be determined. In many cases, only upper limits can be given. In addition, there may be hidden bursts not observed with GRB satellite experiments. It is therefore not useful to model a detailed distribution of boost factors for GRBs, while the simulation results connecting the spectral index of the spectrum with a boost factor are subject to uncertainty, as is implied by the absence of a monotonic trend in Table 1.

It was shown that for boost factors of $\Gamma > 100$, the source spectra lie between $E_p^{-1.5}$ and $E_p^{-0.7}$. A conservative estimate for the flattened GRB spectra will

be adopted using

$$\frac{d\Phi_{GRB}}{dE_p} \propto E_p^{-1.5}. \quad (13)$$

The situation is simpler for AGN, as the shock's boost factors vary only up to between $\Gamma = 10$ and $\Gamma = 30$ (Biermann and Strittmatter, 1987). Here, all computed spectra cluster around a value of $E_p^{-2.1}$. Therefore, the AGN spectrum will be taken as

$$\frac{d\Phi_{AGN}}{dE_p} \propto E_p^{-2.1}. \quad (14)$$

3.2.2 From CR shock acceleration spectra to a diffuse spectrum

The diffuse spectrum as measured at Earth depends on several factors:

- *Single source spectra at the source* $d\Phi/dE_p$. The spectral behaviour was already discussed in the previous subsection. To account for particle propagation, adiabatic energy losses need to be considered as $E_p(z) = E_p \cdot (1+z)$. Here, $E_p(z)$ is the energy as observed at a source at redshift z and E_p is the corresponding energy observed at Earth. Diffusive propagation in the magnetic field between clusters is assumed to involve only small angle scattering with preservation of spectral shape. Anisotropy in the source distribution is neglected. In addition, we consider pure proton spectra so that spallation effects are not present.
- *Source evolution* $g(z)$: It is assumed that both AGN and GRBs follow the SFR to determine the number density evolution with comoving volume, see for example, Hasinger et al. (2005) in the case of AGN and Pugliese et al. (2000) in the case of GRBs. A large sample of radio quiet AGN selected at X-ray wavelengths was investigated by Hasinger et al. (2005). The comoving density $dn/dV(z)$ is given as

$$\frac{dn}{dV}(z) \propto \begin{cases} (1+z)^m & \text{for } z < z_1 \\ (1+z_1)^m & \text{for } z_1 < z < z_2 \\ (1+z_1)^m \cdot 10^{k \cdot (z-z_2)} & \text{for } z > z_2, \end{cases} \quad (15)$$

with the parameters $m = 5.0$, $z_1 = 1.7$, $z_2 = 2.7$ and $k = -0.43$. The total redshift evolution $g(z)$ further includes multiplying the comoving volume dV/dz with a factor $1/(4\pi d_L^2)$ to account for the decrease of the flux L with the distance d_L , neglecting a possible travel limitation to the distance

reached by significant magnetic scattering. Therefore,

$$g(z) = \frac{dn}{dV}(z) \cdot \frac{dV}{dz} \cdot (4\pi d_L^2)^{-1}. \quad (16)$$

For simplicity, this model is used for both AGN and GRBs. Although deviations between the SFR scenarios of AGN and GRBs are expected, the approximation that both follow the distribution of radio quiet X-ray AGN is reasonable (Hasinger et al., 2005): the deviations being expected to be negligible with respect to general uncertainties arising from assumptions about the acceleration region.

- *Absorption of protons at the highest energies:* Protons at $E_p > 5 \cdot 10^{19}$ eV are absorbed due to interactions with the cosmic microwave background as was recently confirmed by the Auger experiment (Yamamoto et al., 2007). Therefore, the diffuse spectrum resulting from the propagation of a single source spectra is modified by a further factor, $\exp[-E_p/(5 \cdot 10^{19} \text{ eV})]$ to account for this effect.
- *The normalisation of the diffuse spectrum:* Because the calculated particle spectra are given in arbitrary units, normalisation of the overall spectrum as measured at Earth is achieved using observation.
 - In the case of superluminal sources, normalisation of the expected signal follows from the most restrictive upper limit on the neutrino signal from extraterrestrial sources given by the AMANDA experiment, see (Achterberg et al., 2007)

$$E_\nu^2 \frac{dN_\nu}{dE_\nu} < 7.4 \cdot 10^{-8} \frac{\text{GeV}}{\text{s sr cm}^2}. \quad (17)$$

With an average E^{-2} spectrum for both neutrinos and protons, the spectra are connected by assuming that the expected neutrino energy fluence is a fraction q of the proton spectrum

$$\int \frac{dN_\nu}{dE_\nu} E_\nu dE_\nu = q \cdot \int \frac{dN_p}{dE_p} E_p dE_p, \quad (18)$$

with $q = 1/40$, since only 20% of the proton flux goes into pion production via the delta resonance, 1/2 of the remaining flux goes into the charged pion component of which 1/4 goes into neutrinos, see e.g. Becker (2008).

- In the case of subluminal sources, using neutrino flux limits leads to an excess above the observed spectrum of charged CRs, since the limits are not stringent enough yet. Instead, the measured part above the 'ankle' of the CR spectrum is used for an estimate of the contribution from subluminal sources. The CR energy flux above the ankle is given by (Waxman and Bahcall, 1997, 1999)

$$j_E(E_{\min} = 3 \cdot 10^{18} \text{ eV}) := \int_{3 \cdot 10^{18} \text{ eV}} \frac{dN_p}{dE_p} E_p dE_p \approx 10^{-7} \text{ GeV cm}^{-2} \text{ s}^{-1} \text{ sr}^{-1}. \quad (19)$$

It is expected that this contribution comes from a combined signal from AGN and GRBs. In the following it is assumed that the fraction of UHECRs coming from AGN, contributes a fraction $0 < x < 1$. Therefore, the fraction of UHECRs from GRBs is $(1 - x)$.

Thus, the total spectrum as observed at Earth is given as

$$\frac{dN_p}{dE_p} = A_p \int_{z_{\min}}^{z_{\max}} \left(x \cdot \frac{d\Phi_{AGN}}{dE_p}(E_p(z)) + (1 - x) \cdot \frac{d\Phi_{GRB}}{dE_p}(E_p(z)) \right) \cdot g(z) dz. \quad (20)$$

The minimum redshift is set to $z = 0.0018$ as the distance of the closest AGN, Centaurus A. The maximum redshift is taken to be $z_{\max} = 7$. As the main contribution comes from redshifts of $z \sim 1 - 2$ due to the high number of sources at these redshifts, the exact values of the integration limits are not crucial.

3.2.3 Comparison with the observed cosmic ray spectrum

The diffuse spectrum as measured at Earth is shown in Figure 3. Data points represent measurements from a selection of experiments. Our calculated spectra from superluminal and subluminal shocks are displayed as the dashed and solid lines.

It appears from Figure 3, that in the superluminal shock case, the only possible contribution to the measured CR spectrum is around the knee. It is expected, however, that the effective flux is actually even lower, because the normalisation is based upon the assumption that the contribution cannot be more than the current neutrino flux limits permit. Therefore, the calculated flux can be considered as an absolute upper limit. Here, the fraction of AGN protons has been chosen to be $x=0.5$, assuming that 50% of the signal is produced by AGN and 50% by GRB

The subluminal shock case has been investigated for different scenarios. The upper line represents a spectrum that would be produced by AGN only ($x = 1$). The lower line represents a pure GRB spectrum ($x = 0$). The flux is too low to explain the observed component above the ankle if a significant contribution comes from GRBs because of the flatness of the GRB spectra. It seems that the flat spectra do not fit the present observations. Thus, AGN are the favoured sources for the production of UHECRs. Figure 4 shows the CR spectrum at the highest energies, multiplied by $E^{2.7}$ in order to have a clearer view on the features of the spectrum. The upper and lower solid lines represent the same predictions for shocks as in Fig. 3. The middle line assumes that 50% is made up by AGN and the remaining 50% comes from GRBs. The normalisation fits the HiRes data. There is a discrepancy between the

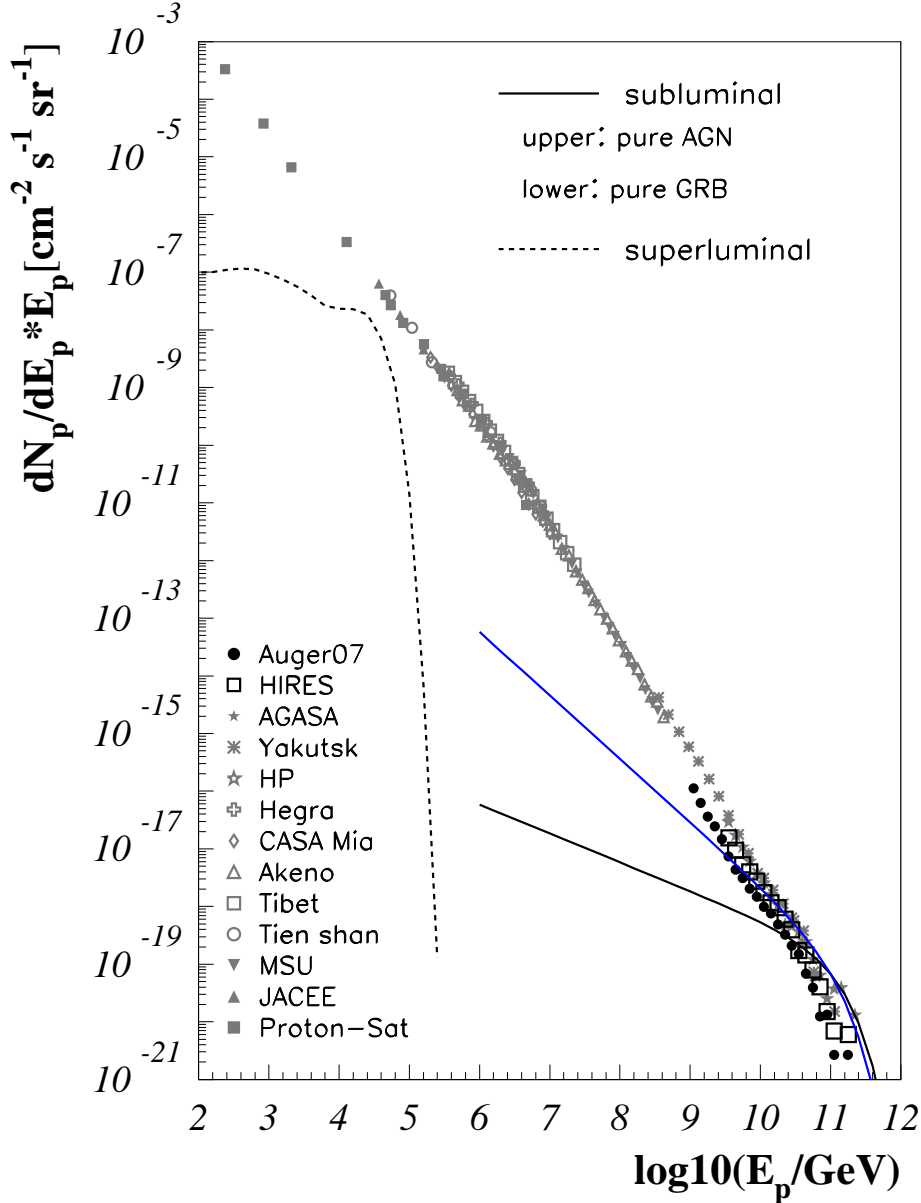


Fig. 3. The maximum predicted diffuse flux from GRBs and AGN with superluminal shock fronts (dashed line) and subluminal shocks (solid lines). For subluminal sources, the upper line is a pure AGN-produced spectrum, the lower line represents a pure GRB spectrum. The flux is compared to the measured CR spectrum. Data points are taken from the different experiments: Auger – Yamamoto et al. (2007); HiRes – The High Resolution Fly’s Eye Collaboration (2002); AGASA – Yoshida et al. (1995); Yakutsk – Krasilnikov et al. (1985); Haverah Park – Ave et al. (2001); HEGRA – Aharonian et al. (1999); CASA-MIA – Glasmacher et al. (1999); Akeno – Krasilnikov et al. (1985); Tibet – Ozawa et al. (2003); Tien Shan – Antonov et al. (1995); MSU – Khristiansen et al. (1994); JACEE – Asakimori et al. (1995); Proton-Sat – Grigorov et al. (1975); KASCADE – Antoni et al. (2005). In the case of superluminal sources, 50% is assumed to come each from GRB and from AGN.

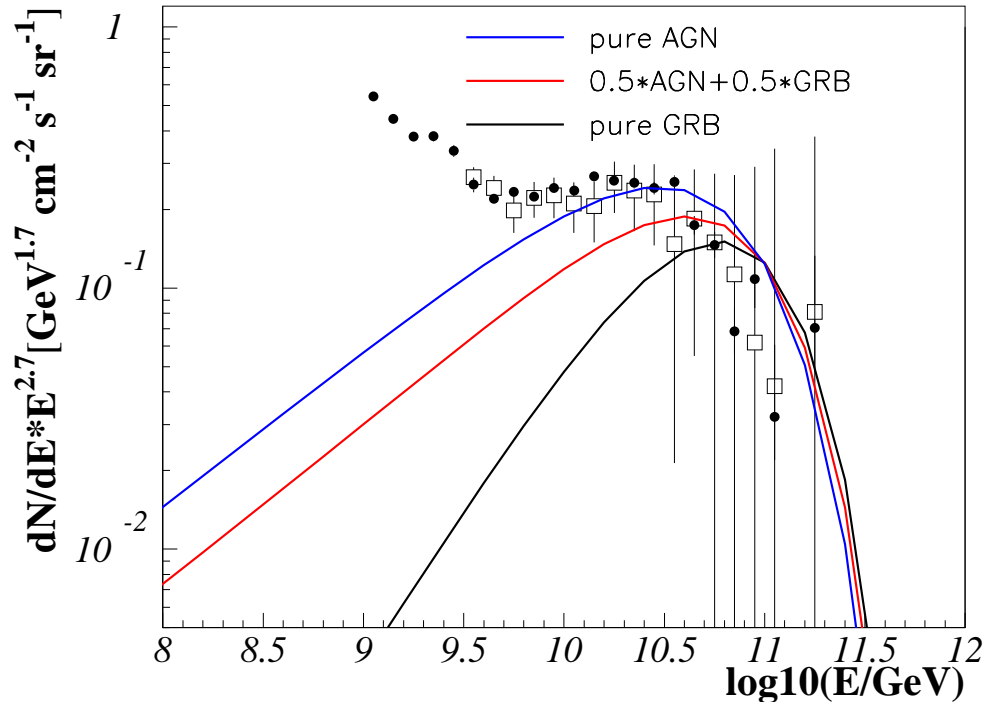


Fig. 4. Spectrum of UHECRs multiplied by $E^{2.7}$. Data points from Auger (Yamamoto et al., 2007) and HiRes (The High Resolution Fly’s Eye Collaboration, 2002). The solid lines represent the same predictions as presented in Fig. 3. Auger data have been renormalised at $10^{10.3}$ GeV to HiRes data and the calculated spectra have also been normalised to HiRes data. The data can be described well by a pure AGN spectrum (blue line) within experimental uncertainties and test particle acceleration accuracy. The red line is a mixture of 50% GRB contribution and 50% AGN contents, the black line is a pure GRB spectrum. Both do not fit the data.

normalisation of HiRes and Auger data, which is not entirely understood yet, but is probably due to systematic errors in the energy and flux determination of the experiments. Therefore, the Auger data are renormalised at $10^{10.3}$ GeV to match the normalisation of the HiRes data. With an assumed significant contribution from GRBs, it seems difficult to explain the observed spectrum. Within the uncertainties of the experimental data, our predicted spectra fit the measured spectra between $10^{9.8}$ GeV and $10^{10.5}$ GeV if pure AGN spectra are assumed. The flux is slightly too low for the first data points above the ankle, between $10^{9.5}$ GeV and $10^{9.8}$ GeV. The steepening of the spectrum at lower energies cannot be due to some contribution from sources with a high field inclination to the normal because we have shown that such superluminal shocks cannot produce energies above about $10^{10.5}$ GeV. It is possible that the steepening arises from the addition of subluminal sources with varying maximum energy, determined by varying maximum field strengths, so only

a fraction of the sources reach the highest energies of 10^{21} eV. Ahlers et al. (2005), fitting HiRes data to a cosmological source distribution similar to ours in Section 3.2.2, find some steepening around 10^9 GeV due to details of the photo-production propagation function. While these effects suffice to explain the small difference for the lowest energies above the ankle concerning AGN spectra, they cannot explain the large differences between the data and the GRB spectral predictions.

4 Implications for high energy neutrino and photon astronomy

Fig. 3 has an interesting implication for neutrino and TeV-photon astronomy. Neutrinos and TeV photons are produced in proton-photon or proton-nucleon interactions, see e.g. Becker (2008) for a review,

$$p\gamma \longrightarrow \Delta^+ \longrightarrow \begin{cases} p\pi^0 & , \text{fraction } 2/3 \\ n\pi^+ & , \text{fraction } 1/3 \end{cases} \quad (21)$$

$$pp \longrightarrow \pi^+ \pi^- \pi^0. \quad (22)$$

The decay of the π^0 leads to high energy photon emission, and π^\pm particles produce neutrinos. The photon signal at TeV energies is not unique, since leptonic processes like Inverse Compton scattering contribute at the same energies. Therefore, the best, unambiguous way of identifying the hadronic interactions are neutrino observations.

Models for neutrino emission in AGN are present in e.g. Mannheim (1995); Mannheim et al. (2001); Stecker (2005); Becker et al. (2005), where it is assumed that protons accelerated in AGN jets can interact with different photon fields to produce neutrinos.

Proton-photon interactions in the prompt phase of GRBs can lead to neutrino and TeV-photon production. In the first approach by Waxman and Bahcall (1997, 1999), it is assumed that GRBs are the sources of UHECRs to calculate the neutrino spectrum. According to our results in the previous sections, GRBs are unlikely to be the sources of UHECRs and the model does not hold anymore. However, further developments of the model normalize the flux to the electromagnetic output rather than to the flux of UHECRs, see e.g. Guetta et al. (2004); Becker et al. (2006); Murase and Nagataki (2006). Here, the protons do not need to be accelerated to the highest energies: The photon field of the prompt emission of GRBs has characteristic energies of around ~ 100 keV–1 MeV, and can reach energies up to > 100 MeV, see e.g. (Schneid et al., 1992; González et al., 2003; Hurley et al., 1994). The pro-

ton energy necessary to produce a Delta resonance, and with this TeV-photons and neutrinos, is given as

$$E_p \geq \frac{\Gamma^2}{(1+z)^2} \frac{m_\Delta^2 - m_p^2}{4} \cdot E_\gamma. \quad (23)$$

Here, m_Δ is the mass of the Delta resonance, m_p is the proton's mass, z is the redshift of the source and E_γ is the characteristic photon energy. The proton energy required for the process is therefore given as

$$E_p \geq 5 \cdot 10^7 \cdot (1+z)^{-2} \cdot \left(\frac{\Gamma}{100}\right) \cdot \left(\frac{E_\gamma}{1 \text{ MeV}}\right)^{-1} \text{ GeV}. \quad (24)$$

Thus, with redshifts typically of the order of $z = 1$ and boost factors of around $\Gamma = 300$, the proton energy sufficient for neutrino and TeV-photon production is as low as

$$E_p \sim 10^6 \text{ GeV}. \quad (25)$$

This opens the possibility of neutrino production from sources which are *not* observable in charged UHECRs. While the lower energy spectra of extragalactic, charged cosmic rays cannot be observed due to the high galactic background, neutrinos may serve to investigate those sources further.

Using the same reasoning as above, we can conclude that charged UHECRs from *superluminal* spectra may not be observed in charged cosmic rays, but are good candidates for the production of high energy neutrinos and photons from AGN or GRBs. Those shocks may produce low energy spectra of much higher intensity than subluminal shocks, which are simply hidden due to the galactic background. Neutrinos and photons, on the other hand, point back to the original source, and may be identified. We can use the maximum energy of the proton spectra to calculate the energy of the photon spectra which are necessary to produce high energy photons and neutrinos by using Equ. (23),

$$E_\gamma \geq \frac{\Gamma^2}{(1+z)^2} \frac{m_\Delta^2 - m_p^2}{4} \cdot E_p \quad (26)$$

$$= 5 \cdot 10^7 \cdot (1+z)^{-2} \cdot \left(\frac{\Gamma}{100}\right) \cdot \left(\frac{E_p}{1 \text{ GeV}}\right)^{-1} \text{ MeV}. \quad (27)$$

For mildly relativistic shocks of $\Gamma \sim 10$ as they occur in AGN, superluminal proton spectra reach up to $E_p \sim 100 \text{ GeV}$. This requires photon energies of $E_\gamma \geq 10 \text{ GeV}$. These high energies can be produced by Inverse

Compton scattering of synchrotron or external photons with the accelerated electrons. A catalog of AGN with photon emission above 100 MeV was already presented by the EGRET experiment (Sreekumar et al., 1998), and more sources are likely to be identified when GLAST is launched this summer (Gehrels and Michelson, 1999).

Highly relativistic shocks with $\Gamma > 100$ reach up to proton energies of 10^5 GeV. This requires photon energies of $E_\gamma \geq 100$ MeV. This is about 2 orders of magnitude above the characteristic energy, but the photon spectrum is likely to extend to energies above 100 MeV as already observed for more than 30 GRBs, see e.g. (Schneid et al., 1992; González et al., 2003; Hurley et al., 1994). If mildly relativistic internal GRB shocks are to contribute to neutrino production, photon energies in excess of 1 GeV are required. Such sources would also need to be insignificant producers of UHECRs, to satisfy the discussion of Section 3.2.2.

In conclusion, low energy proton spectra from extragalactic sources cannot be observed directly due to the high galactic background of cosmic rays, but they may be detected indirectly by means of high energy neutrino and photon spectra.

5 Summary & conclusions

In this work we have presented Monte Carlo simulation studies of the acceleration of test particles in relativistic, subluminal and superluminal shock environments. The source candidates discussed were AGN jets with mildly-relativistic shocks of boost factors of $\Gamma \approx 10 - 30$ and GRBs regions with highly-relativistic shocks, $100 < \Gamma < 1000$. The resulting particle spectra were used to calculate a contribution to the diffuse CR spectrum.

Particle spectra have been obtained with varying the shock boost factor Γ and shock obliquity, i.e. the inclination angle between the shock normal and the magnetic field, ψ . Only subluminal shocks are efficient enough to accelerate particles up to 10^{12} GeV, while superluminal shocks are effective up to $\sim 10^5$ GeV. Flat spectra are found for very high subluminal shock boost factors, but for superluminal shocks the spectral indices stay roughly constant between values of 2.0 to 2.3 in the limited region of efficient acceleration, before a cutoff sets in. For the subluminal shock cases, the spectra for mildly-relativistic shocks have spectral indices around 2.0 – 2.2. Highly-relativistic shocks have spectra as flat as $E_p^{-0.7} - E_p^{-1.5}$ at energies between $10^{9.5}$ GeV and $10^{10.5}$ GeV. There is no universal spectral form, rather a variety of spectral shapes with a noticeable plateau-like structure developing at higher Γ values. This structure is very probably related to the number of scattering cycles undergone by particles

at a particular energy.

Our results can be summarised as follows:

- (1) Subluminal shock studies with the pitch scattering angle determined to lie in the range $1/\Gamma \leq \delta\theta \leq 10/\Gamma$, approximately correspond to a situation with a spectrum of scattering waves, $P(k) B^2 = 5/4/\sqrt{2} \cdot \Gamma^{-2} \cdot k^{-1}$ and with the neglect of cross-field diffusion. The resulting spectral slopes were roughly independent of inclination angle, though details of the features were different. A dependence of the spectral index α_p on the shock boost factor Γ was found, leading to spectra of $\alpha_p \sim 2.0 - 2.1$ for mildly-relativistic shocks of $\Gamma \sim 10 - 30$, but producing much harder spectra ($0.7 < \alpha_p < 1.5$) for highly-relativistic shocks, $100 < \Gamma < 1000$.
 The above implies that GRB particle spectra arising from relativistic shocks with very high boost factors between $100 < \Gamma < 1000$, have spectra flatter than $E_p^{-1.5}$, much flatter than AGN spectra, $\sim E_p^{-2}$. Moreover, the above findings are supported by the lower Γ work of Niemec and Ostrowski (2005) and Stecker et al. (2007). Observational evidence, (Dingus, 1995), regarding irregular and flat spectra from GRBs may be explained by the spectra we present. This work is also consistent with the general observations of the electron spectra that may be injected from the terminal hotspots to the lobes of the powerful FR-II radio galaxies which are not of a single and universal power-law form, as shown in detail in Rudnick et al. (1994), Machalski et al. (2007), etc.
- (2) Superluminal shocks are only efficient in accelerating CRs up to $E_p \sim 10^5$ GeV, resulting in spectral indices of $\alpha_p \sim 2.0 - 2.3$. On the other hand, subluminal shocks are more efficient and able to accelerate CRs up to $E_p \sim 10^{12}$ GeV, factors of 10^{9-11} above the particle injection energy.
- (3) We discussed the possible contributions of AGN and GRBs to the UHECR flux. For superluminal sources, such contributions can be excluded using current neutrino flux limits to normalise the spectrum. In the case of subluminal sources, the spectrum is normalised to the CR flux above the ankle, $E_{\min} = 10^{9.5}$ GeV. Using only AGN ($\Gamma = 10$), the spectrum fits the data within experimental uncertainties. With a significant contribution from the very high relativistic shocks in GRBs ($100 < \Gamma < 1000$), however, the total spectrum is too flat and it is difficult to explain the lower part of the spectrum around $E_p \sim 10^{9.5}$ GeV. Even if UHECRs are accelerated in either external or internal shocks of GRBs, it is necessary to account for all the energy in accelerated particles, down to the injection energy. The total relativistic plasma output available from GRBs is only marginally sufficient to account for the total energy required in the extra-galactic CR spectrum.
- (4) Recent Auger results indicate a correlation between CRs at the highest energies ($E_p > 5.7 \cdot 10^{10}$ GeV) and the distribution of AGN (The Pierre Auger Collaboration, 2007). This is a first evidence that the cosmic ray flux *above* the GZK

cutoff originates from AGN predominantly in the supergalactic plane. The question of the origin of CRs *below* the GZK cutoff is not answered by this observation, but it is likely that more distant AGN contribute significantly to the flux, as AGN in the supergalactic plane make up the flux *above* the GZK cutoff. Moreover the output of X-ray active AGN within 60 Mpc provides an energy density exceeding the local estimated total extra-galactic CR energy density by a factor 10^4 . It therefore seems reasonable to believe that the results from Auger can be explained by subluminal relativistic shock acceleration in AGN. It is now important to further develop the simulation results by including particle interactions, more detailed modelling of particle propagation in the inter-galactic medium and by investigating the source distribution of AGN in relation to observation in order to resolve the question of which AGN are the main sources of UHECRs.

- (5) Extragalactic, superluminal shocks are good candidates for the production of high energy neutrinos and photons. The energy density at low energies may be quite high compared to the observed flux of UHECRs, but hidden by galactic cosmic rays. Neutrino- and photon fluxes may, on the other hand, be identified and are probably the only possibility to observe extragalactic, superluminal shocks.

Acknowledgements

We are grateful to Peter Biermann, Francis Halzen and Wolfgang Rhode for extensive and fruitful discussions on this work. The project was co-funded by the European Social Fund and National Resources (EPEAEK II) PYTHAGORAS, Greece.

A The simulation

The use of a Monte Carlo technique to solve Equ. (5) is dependent on the assumption that the collisions represent scattering in pitch angle and that the scattering is elastic in the fluid frame where there is no residual electric field. Since we assume that the Alfvén waves have lower speed than the plasma flow itself, the scattering is elastic in the fluid frame. A phase averaged distribution function is appropriate to the diffusion approximation we employ which uses many small angle scatters.

We begin the simulation by injecting 10^5 particles far upstream and of a weight w_p equal to 1.0. A splitting technique is used similar to the one used in the Monte Carlo simulations of Meli and Quenby (2003a,b), so that when an energy level is reached such that only a few accelerated CRs remain, each particle is replaced by a number of N particles of statistical weight $1/N$, so as to keep a roughly constant number of CRs followed. First order Fermi (diffusive) acceleration is then simulated by following the particles' guidance centres and allowing for numerous pitch angle scatterings in interaction with the assumed magnetised media, while at each shock crossing the particles gain an amount of energy determined by a transformation of reference frame. The particles are assumed to be relativistic with an initial injection energy of $\gamma \sim (\Gamma + 100)$ when they are entered in the model upstream directed towards the shock. As a justification for a test particle approach, we note that Bell (1978a,b) and Jones and Ellison (1991) have shown that 'thin' sub-shocks appear even in the non-linear regime, so at some energy above the plasma Γ value, the accelerated particles may be dynamically unimportant while they re-cross the discontinuity. Another way of arriving at the test-particle regime is to inject particles well above the plasma particle energy when they are dynamically unimportant and thus require the seed particles to have already been pre-accelerated.

The basic coordinate system employed to describe a shock is a Cartesian system (x, y, z) , where the shock plane lies on the (y, z) plane. The reference frames used during the simulations are the upstream and downstream fluid frames, the normal shock frame (NSH) and the de Hoffmann-Teller (HT) frame, see Figures A.1 and A.2.

For the oblique shock cases studied here, provided the field directions encountered are reasonably isotropic in the shock frame, we know that $\tan \psi_1 = \Gamma_1^{-1} \tan \psi_{NSH} \sim \Gamma_1^{-1} \sim \psi_1$ where '1' and 'NSH' refer to the upstream and normal shock frames respectively. The concentration of field vectors close to the x -axis in the upstream fluid frame allows for a reasonable probability of finding a de Hoffmann-Teller frame with a boost along the negative y -axis less than c . Making this boost then yields an upstream HT frame inclination,

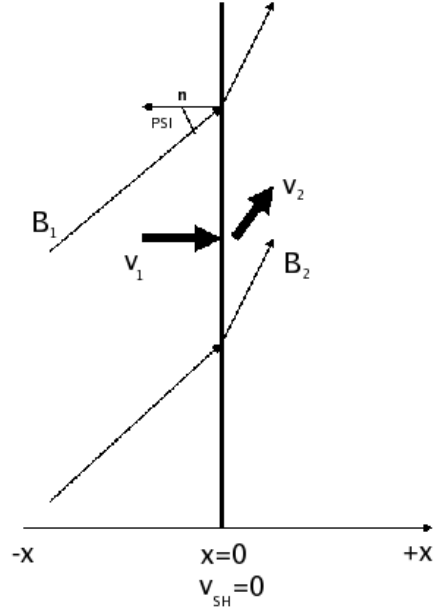


Fig. A.1. The coordinate system of a shock as seen in the so called (normal) shock frame.

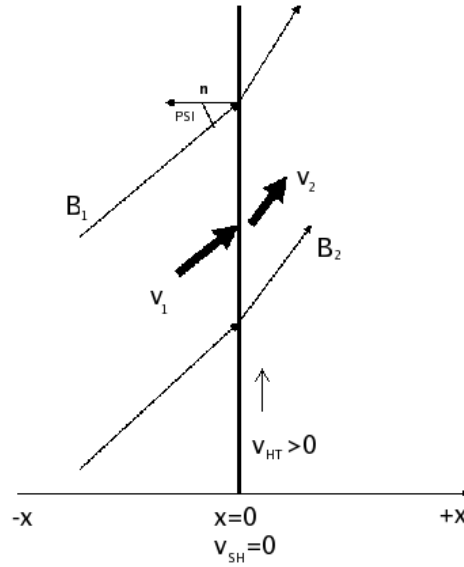


Fig. A.2. The coordinate system of a shock as seen in the so called de Hoffmann and Teller frame.

$\tan \psi_{HT,1} = \Gamma_{HT,1} \tan \psi_1$. While all particles are allowed to cross from downstream to upstream, only particles with a critical HT frame pitch angle, θ_c , given by

$$\theta_c = \arcsin\left(\frac{B_{HT,1}}{B_{HT,2}}\right)^{0.5} \quad (\text{A.1})$$

are allowed to cross down to upstream and conservation of the first adiabatic invariant is used to determine the new, downstream pitch angle. A compression ratio of 3 is used although some MHD conditions favour a value of 4. Meli and Quenby (2003b) do not find a considerable difference in simulation results between these two cases. The results of Newman et al. (1992) suggest that it is legitimate to use Equ. A.1 as a reasonable approximation. These authors checked the preservation of the first adiabatic invariant for the worst case, near perpendicular shock, employing trajectory integration with a realistic scattering field right up to the shock interface. At the critical angle for a compression ratio of three shock, adiabatic invariant deviations were typically confined within ten percent while large effects tended to occur only towards 90 degree pitch angle. Particles are assigned a random phase so that a 3-dimensional transformation of momentum vectors can be achieved between the fluid and HT frames. Away from the shock, the guiding centre approximation is used so that a test particle moving a distance, d , along a field line at ψ to the shock normal, in the plasma frame has a probability of collision within d given by $P(d) = 1 - \exp(-d/\lambda) = R$, where the random number R is $0 \leq R \leq 1$. Weighting the probability by the current in the field direction μ yields $d = -\lambda\mu \ln R$. The pitch angle is measured in the local fluid frame, while the value x_i gives the distance of the particles to the shock front, where the shock is assumed to be placed at $x = 0$. Furthermore, x_i is defined in the shock rest frame and the model assumes variability in only one spatial dimension. Scattering in pitch is applied as described in the main body of this text.

In our simulations continuous Lorentz transformations are performed from and into the local plasma frames into or from the shock frame in order to check for particle shock crossings. All particles leave the system if they escape far downstream at the spatial boundary, r_b . The downstream spatial boundary required can be estimated initially from the solution of the convection-diffusion equation in a non-relativistic, large-angle scattering approximation in the downstream plasma, which gives the chance of return to the shock as $\exp(-V_2 r_b / x_i)$. In fact, we have performed many runs with different spatial boundaries to investigate the effect of the size of the acceleration region on the spectrum, so as to find a region where the spectrum is size independent. Alternatively, the particles leave the system if they reach a specified maximum energy E_{\max} for computational convenience.

For the superluminal shock conditions, where the physical picture of the shock drift acceleration applies, it is necessary to abandon the guiding centre approximation when the trajectories begin to intersect the shock surface. Here, we consider a helical trajectory motion of each test-particle of momentum p , in the fluid frame, upstream or downstream, where the velocity coordinates

(v_x, v_y, v_z) of the particle are calculated in 3-dimensional space as follows

$$v_{x_i} = v_i \cos \theta_i \cos \psi_i - v_i \sin \theta_i \cos \phi_i \sin \psi_i, \quad (\text{A.2})$$

$$v_{y_i} = v_i \cos \theta_i \sin \psi_i + v_i \sin \theta_i \cos \phi_i \cos \psi_i \quad (\text{A.3})$$

and

$$v_{z_i} = -v_i \sin \theta_i \sin \phi_i. \quad (\text{A.4})$$

Here, θ_i is the pitch angle, $\phi_i \in (0, 2\pi)$ and ψ_i is the angle between the magnetic field and the shock normal in the respective fluid frames ($i=1,2$ for upstream and downstream respectively).

We follow the trajectory in time, using $\phi_i = \phi_o + \omega t$, where t is the time from detecting shock presence at x_{NSH} , y_{NSH} , z_{NSH} by using

$$dx = x_{NSH} + v_{x_i} \delta t, \quad (\text{A.5})$$

$$dy = y_{NSH} + v_{y_i} \delta t \quad (\text{A.6})$$

and

$$dz = z_{NSH} + v_{z_i} \delta t \quad (\text{A.7})$$

assuming that $\delta t = r_g/Hc$ where $H \geq 100$ and r_g is the Larmor radius. The particle's gyrofrequency ω is given by the relation, $\omega_i = e|\vec{B}_i|/\gamma_i$, \vec{B}_i is the magnetic field, γ_i is the particle's boost factor and e is its charge in gaussian units.

We follow the helical trajectory of each particle in time t , in the new frame where t is the time from detecting the shock intersection at (x, y, z) until the trajectory has performed one gyro period without re-intersecting the shock surface. Nevertheless, because of the peculiar properties of the helix we need to establish where a particle, starting off in the upstream frame, with a particular θ and ϕ first encounters the shock. To establish when the shock encounter happens, we choose to go back a whole period, $T_i = 2\pi/\omega_i$ by reversing signs of the helix velocity coordinates and by keep checking throughout the simulation to determine if the particle trajectory encounters the shock front, placed at $x = 0$ in the shock rest frame. If the particle encounters the shock then the suitable Lorentz transformation to the relevant fluid rest frame is made and we continue following the particle helical trajectory until shock intersections cease. At this juncture, the guiding centre is followed in the same way as in the diffusive acceleration picture of the subluminal shocks. During the helical

phase of the numerical integration, the prescription for pitch angle scatter is applied as in the general plasma frame motions, in order to more realistically simulate a mean plus chaotic field situation where turbulence is clearly present close to a shock.

B The spectra

The particle spectra resulting from the simulation are presented in Figures B.1, B.2 and B.3. In each of the figures, the simulated particle spectra are shown (black dots) for three different shock angles each, $\psi = 23^\circ, 33^\circ, 43^\circ$, for nine different boost factors, $\Gamma = 10, 20, 30$ in the first row, starting from the left, $\Gamma = 100, 300, 500$ in the middle row and $\Gamma = 700, 900, 1000$ in the lower row. Each graph shows the logarithm of the proton spectrum $d\Phi/dE_p$ in arbitrary units versus the proton's energy in units of GeV. Note that the spectrum can be expressed more generally in terms of the particle's boost factor $\gamma = E_p/(m_p c^2)$. Therefore, the results are also valid for nuclei with higher mass (e.g. Fe). In the present investigation protons are considered.

Figures B.1, B.2 and B.3 show that the spectral shape starts to deviate from a power-law as Γ increases with the onset of plateau formation. This might be expected, since the particles are swept away rapidly downstream with a low possibility to return upstream for high Γ factors (around 20% of the particles return to the shock after one shock cycle). A small chance to return to the shock (except for a relatively small subset of downstream pitch angle particle 'histories') produces the spectral irregularities and the anisotropy seen for these returning particles. We note that in the cases of $\Gamma = 10 - 30$ relatively smooth spectra are produced, but spectra become more structured (plateau-like) at the more extreme values $\Gamma \rightarrow 1000$. In the latter cases the effects of individual acceleration cycles are clearly evident. The mechanism of plateau development as an acceleration cycle effect is implicit in figure 6 of Protheroe (2001) and figure 2 of Stecker et al. (2007) and seems to be independent of the shock inclination angle for a particular scattering model. The structured spectra can also be seen in the lower Γ large angle scatter model simulations of Quenby and Lieu (1989) and Ellison et al. (1990) while Protheroe (2001) shows a similar contrast in behaviour, between large and small angle scattering models up to $\Gamma = 20$.

The initial bump in most of the spectra is due to the monochromatic injection of the particles. We approximate the spectra with a power-law (straight lines seen in the figures) at higher energies and thus, artificial injection features are excluded from the calculations. The maximum energy is chosen to be 10^{21} eV as discussed in Section 1.2. The plateau-like parts in the spectra at higher energies are physical features, especially at high boost factors, as particles

continue to be accelerated in a second cycle. The lower energy part of the spectrum is dominated by particles undergoing one acceleration shock cycle, while the second bump in the spectrum represents particles having completed two cycles. A shock cycle is a shock crossing from upstream to downstream to upstream. Since some upstream particles can suffer reflection before downstream transmission, this effect increases the statistical energy gain of the particles in their overall encounter with the shock surface. The aim of fitting a single power-law to the computed spectral points is primarily to examine the variation of primary spectra with the Γ factor of the shock. The spectral points themselves are difficult to compare because the structure becomes more complex with the increasing boost factor. As discussed in the main text, the relevant way to compare the particle spectra to the data is to fit the energy range observed in cosmic rays. The straight lines in Figures B.1, B.2 and B.3 together with the values written in the lower left corner of each graph indicate the single power-law for comparison chosen individually for each case.

Table B.1 shows the spectral index dependence of the boost factor for the three shock inclination angles $\psi = 23^\circ, 33^\circ, 43^\circ$. For each of the three angles, the spectra become harder with the increasing Γ factor of the shock. Due to the structure in the spectra, these values represent simple first order approximations which are useful for comparison of the simulation results with the data. CR data include large statistical and systematic errors, which would make it difficult to distinguish features attributable to the acceleration mechanism other than single or broken power-laws.

The spectral flattening with higher Γ , implies that GRB particle spectra, arising from relativistic shocks with very high boost factors between $100 < \Gamma < 1000$, have spectral indices ranging between $\alpha_p \sim 2.1 - 1.5$. These spectra tend to be somewhat steeper than some particular entries in Table B.1, but the tendency of a flattening with the boost factor is always present. The relativistic flattening effect is consistent with studies of Baring (1999, 2004); Stecker et al. (2007). On the other hand, for shocks with $\Gamma \sim 10 - 30$ occurring in AGN, spectral indices have values between $2.0 < \alpha_p < 2.3$.

In addition, as one sees from Table B.1, the single power-law comparison gives comparable values for different angles ψ . Test simulation runs we performed, using a series of values of ψ , follow the same trend as long as the scattering model is fixed. The present results deviate from earlier investigations by Kirk et al. (2000); Ostrowski and Bednarz (2002), which show a saturation of the hardening of the spectra with the boost factor, $\alpha_p \rightarrow 2.33$ for $\Gamma \rightarrow \infty$. Nevertheless, the latter studies concern the special cases of extremely small values for pitch angle scattering, for particle acceleration in relativistic shocks.

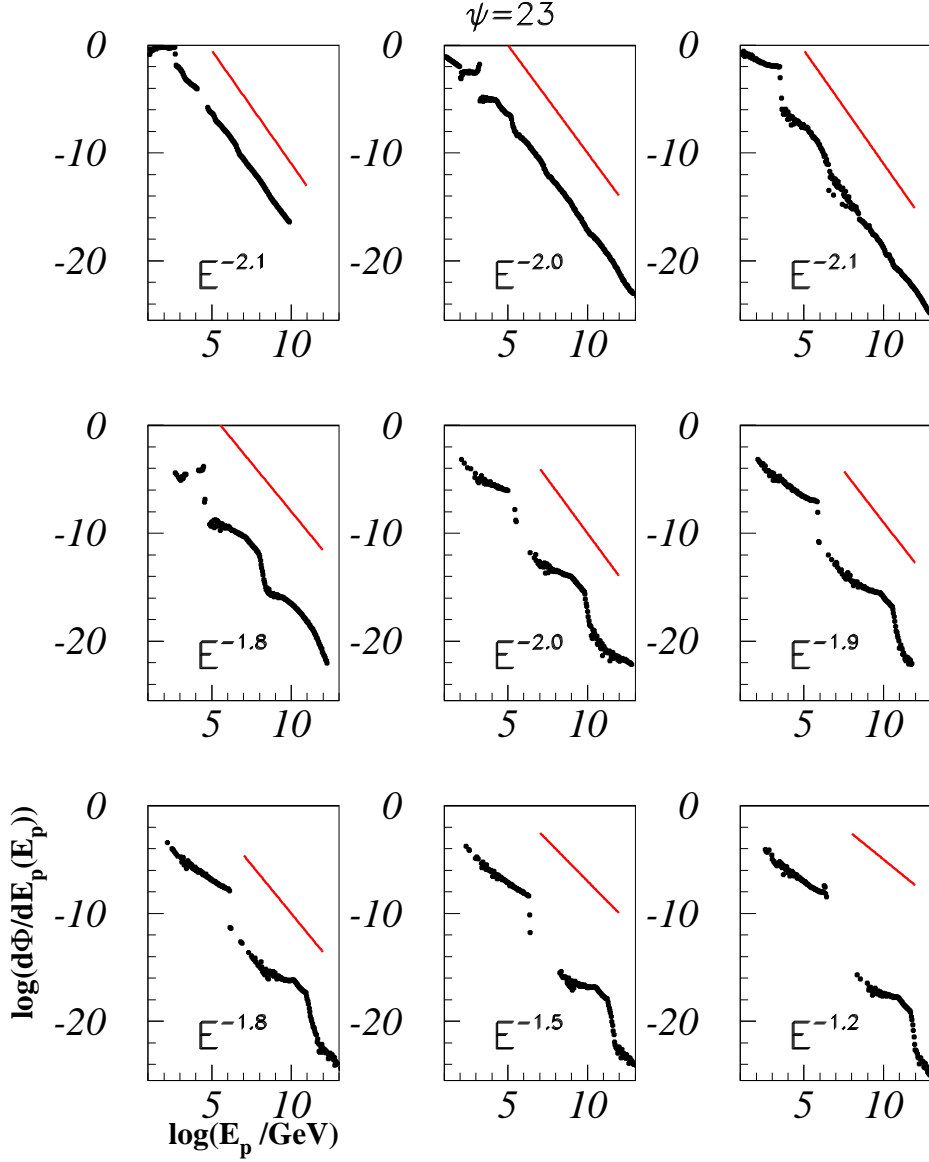


Fig. B.1. Subluminal spectra for $\psi = 23^\circ$ and different Γ : $\Gamma = 10, 20, 30$ is displayed in the first row, in the middle, $\Gamma = 100, 300, 500$ is shown and $\Gamma = 700, 900, 1000$ is the bottom row. The black dots in each graph represent the simulation result. The straight line shows the single power-law for comparison. The spectral behaviour is indicated in the lower left corner of each graph.

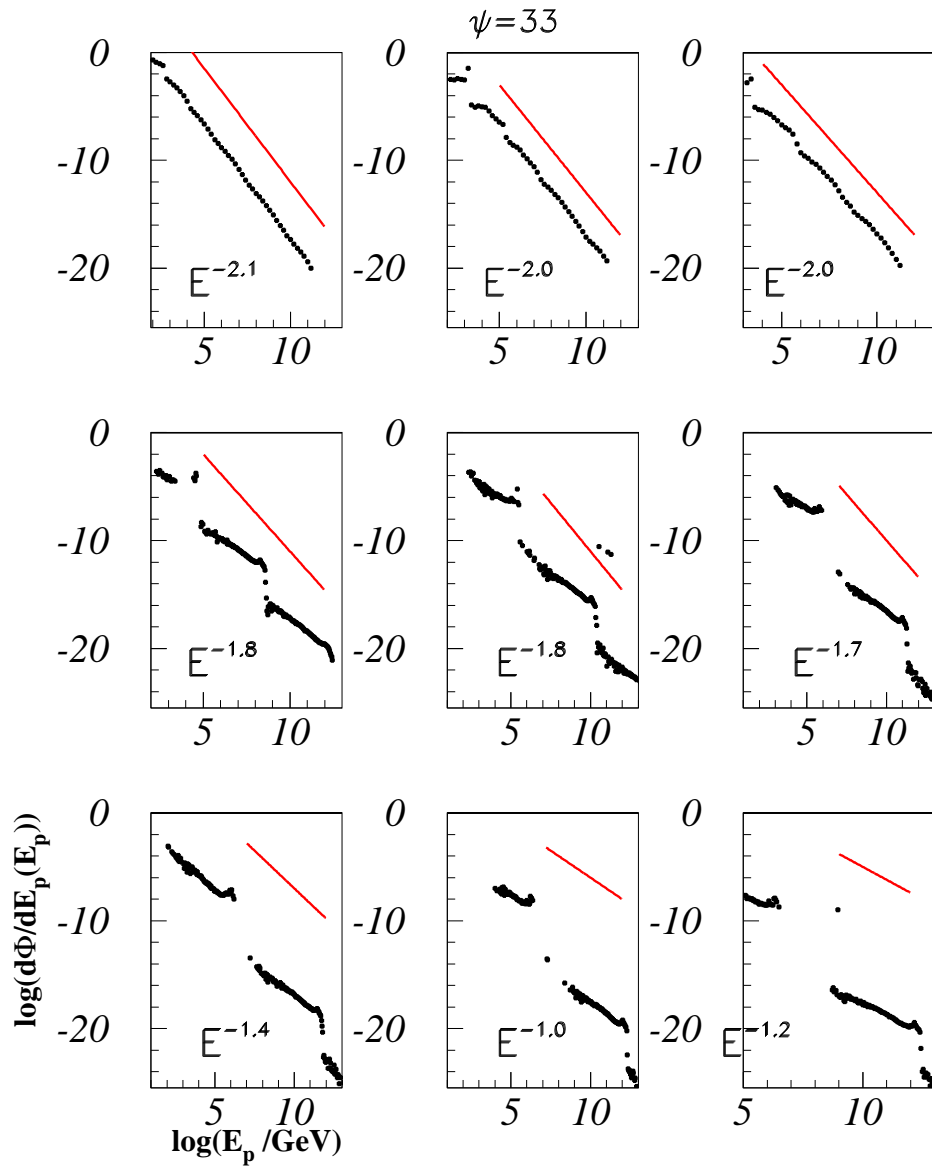


Fig. B.2. Subluminal spectra for $\psi = 33^\circ$ and different Γ , as in Fig. B.1.

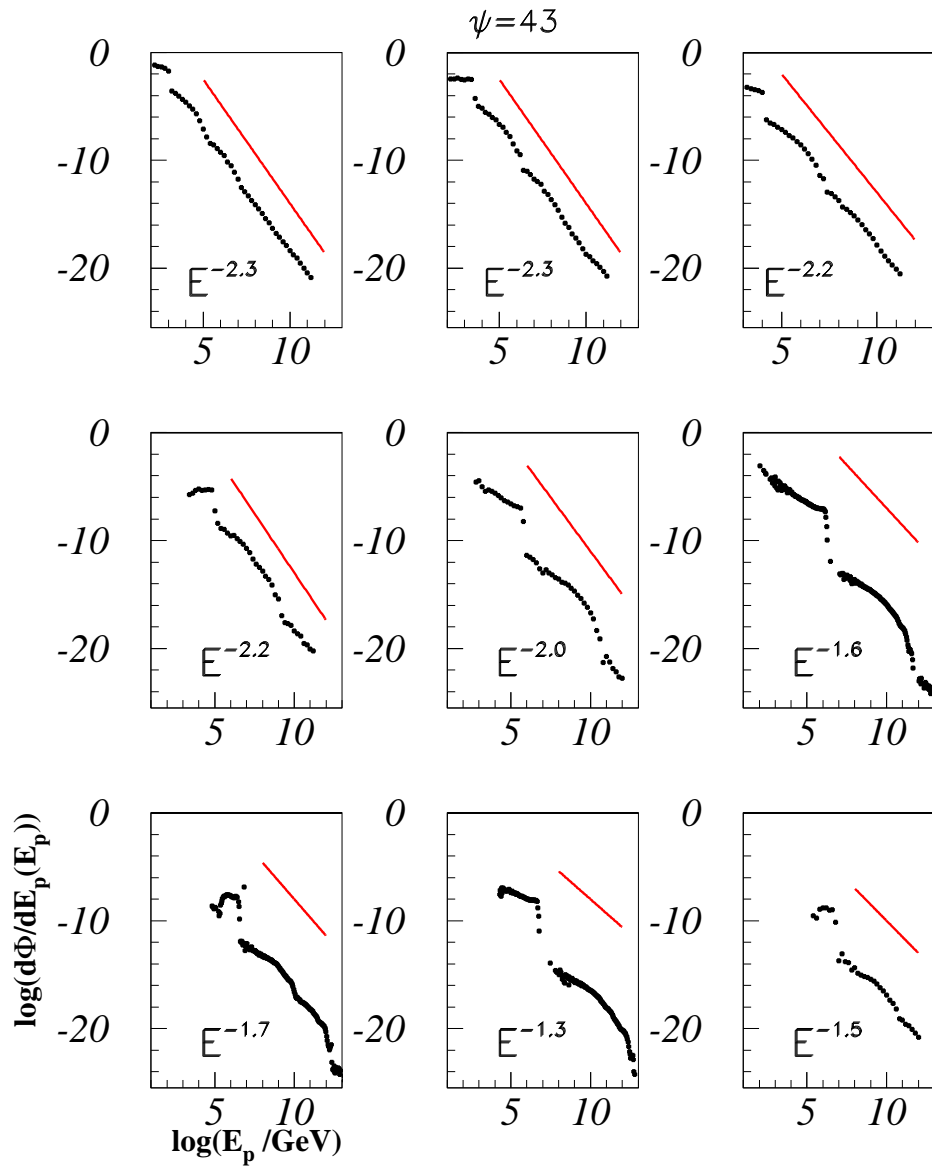


Fig. B.3. Subluminal spectra for $\psi = 43^\circ$ and different Γ , as in Fig. B.1.

Γ	$\alpha_p(\psi = 23^\circ)$	$\alpha_p(\psi = 33^\circ)$	$\alpha_p(\psi = 43^\circ)$
10	2.1	2.1	2.3
20	2.0	2.0	2.3
30	2.1	2.0	2.2
100	1.8	1.8	2.2
300	2.0	1.8	2.0
500	1.9	1.7	1.6
700	1.8	1.4	1.7
900	1.5	1.0	1.3
1000	1.2	1.2	1.5

Table B.1

Spectral indices for a single power-law comparison for subluminal shocks of different boost factors and three inclination angles.

References

- Achterberg, A., et al., 2007. *Phys. Rev. D* 76, 042008.
- Aharonian, F., et al., 1999. *Phys. Rev. D* 59 (9), 092003.
- Ahlers, M., et al., 2005. *Phys. Rev. D* 72 (2), 023001.
- Antoni, T., et al., 2005. *Astropart. Physics* 24, 1.
- Antonov, R. A., et al., 1995. *Astropart. Physics* 3, 231.
- Asakimori, K., Burnett, H. T., et al., 1995. In: *International Cosmic Ray Conference*. p. 707.
- Ave, M., et al., 2001. In: *27th International Cosmic Ray Conference*. p. 381.
- Baring, M., 1999. In: *International Cosmic Ray Conference*. Vol. 4 of *International Cosmic Ray Conference*. p. 5.
- Baring, M. G., 2004. In: *Bulletin of the American Astronomical Society*. Vol. 36. p. 942.
- Becker, J. K., 2008. *Physics Reports* 458 (4-5), 173.
- Becker, J. K., Biermann, P. L., Rhode, W., 2005. *Astropart. Physics* 23, 355.
- Becker, J. K., et al., 2006. *Astropart. Physics* 25 (2), 118.
- Bednarz, J., Ostrowski, M., 1998. *Phys. Rev. Lett.* 80, 3911.
- Begelman, M. C., Kirk, J. G., 1990. *Astrophys. J.* 353, 66.
- Bell, A. R., 1978a. *Month. Not. Roy. Astr. Soc.* 182, 147.
- Bell, A. R., 1978b. *Month. Not. Roy. Astr. Soc.* 182, 443.
- Biermann, P. L., Strittmatter, P. A., 1987. *Astrophys. J.* 322, 643.
- de Hoffmann, F., Teller, E., 1950. *Phys. Rev.* 80 (4), 692.
- Dingus, B. L., 1995. *Astrophysics and Space Science* 231, 187.
- Ellison, D. C., Double, G. P., 2004. *Astropart. Physics* 22, 323.
- Ellison, D. C., Reynolds, S. P., Jones, F. C., 1990. *Astrophys. J.* 360, 702.
- Falcke, H., Malkan, M. A., Biermann, P. L., 1995. *Astron. & Astrophys.* 298, 375.
- Fermi, E., 1949. *Phys. Rev.* 75 (8), 1169.
- Fermi, E., 1954. *Astrophys. J.* 119, 1.
- Forman, M. A., 1970. *Planetary and Space Science* 18, 25.
- Gallant, Y. A., Achterberg, A., Kirk, J. G., 1999. *Astronomy and Astrophysics Supplement* 138, 549.
- Gehrels, N., Michelson, P., 1999. *Astropart. Physics* 11, 277.
- Glasmacher, M. A. K., et al., 1999. *Astropart. Physics* 10, 291.
- González, M. M., et al., 2003. *Nature* 424, 749.
- Grigorov, N. L., et al., 1975. In: Vernov, S. N., Dorman, L. I. (Eds.), *Cosmic Rays*. p. 227.
- Guetta, D., et al., 2004. *Astropart. Physics* 20, 429.
- Halzen, F., Hooper, D., 2002. *Reports of Progress in Physics* 65, 1025.
- Hasinger, G., Miyaji, T., Schmidt, M., 2005. *Astron. & Astrophys.* 441, 417.
- Hillas, A. M., 1984. *Ann. Rev. Astron. Astrophys.* 22, 425.
- Hudson, P. D., 1965. *Month. Not. Roy. Astr. Soc.* 131, 23.
- Hurley, K., et al., 1994. *Nature* 372, 652.
- Jokipii, J. R., 1987. *Astrophys. J.* 313, 842–846.

- Jones, F. C., Ellison, D. C., 1991. *Space Science Rev.* 58, 259.
- Kennel, C. F., Petscheck, H. E., 1966. *J. Geophys. Res.* 71, 1.
- Khristiansen, G. B., et al., 1994. *Astropart. Physics* 2, 127.
- Kirk, J. G., et al., 2000. *Astrophys. J.* 542, 235.
- Krasilnikov, D. D., et al., 1985. In: Jones, F. C. (Ed.), *International Cosmic Ray Conference*. p. 194.
- Krymskii, G. F., 1977. *Akademiia Nauk SSSR Doklady* 234, 1306.
- Lerche, I., Schramm, D. N., 1977. *Astrophys. J.* 216, 881.
- Machalski, J., et al., 2007. *Astron. & Astrophys.* 462, 43.
- Mannheim, K., 1995. *Astropart. Physics* 3, 295.
- Mannheim, K., Protheroe, R. J., Rachen, J. P., 2001. *Phys. Rev. D* 63, 23003.
- Medvedev, M. V., 1999. *Physics of Plasmas* 6, 2191–2197.
- Meli, A., 2003. Ph.D. thesis, Imperial College of Science, Technology and Medicine, London, UK.
- Meli, A., Quenby, J. J., 2003a. *Astropart. Physics* 19, 637.
- Meli, A., Quenby, J. J., 2003b. *Astropart. Physics* 19, 649.
- Moran, E. C., et al., 2001. *Astrophys. J. Let.* 556, L75.
- Murase, K., Nagataki, S., 2006. *Phys. Rev. D* 73 (6), 063002.
- Newman, P. L., et al., 1992. *Astron. & Astrophys.* 255, 443.
- Niemec, J., Ostrowski, M., 2005. *Geophysical Monograph* 156, AGU, Washington, DC, 59.
- Niemec, J., Ostrowski, M., 2007. In: *30th International Cosmic Ray Conference*.
- Ostrowski, M., Bednarz, J., 2002. *Astron. & Astrophys.* 394, 1141.
- Ozawa, S., (Tibet Asgamma Coll.), et al., 2003. In: *28th International Cosmic Ray Conference*. p. 143.
- Parker, E. N., 1958a. *Phys. Rev.* 109, 1328–1344.
- Parker, E. N., 1958b. *Phys. Rev.* 110, 1445–1449.
- Parker, E. N., 1958c. *Astrophys. J.* 128, 664.
- Parker, E. N., 1965. *Astrophys. J.* 142, 1086.
- Parker, E. N., 1966. *Planetary and Space Science* 14, 371.
- Protheroe, R. J., 2001. In: *27th International Cosmic Ray Conference*. Vol. 6 of *International Cosmic Ray Conference*. p. 2006.
- Pugliese, G., et al., 2000. *Astron. & Astrophys.* 358, 409.
- Quenby, J. J., Lieu, R., 1989. *Nature* 342, 654–656.
- Quenby, J. J., Meli, A., 2005. *Geophysical Monograph* 156, AGU, Washington, DC, 9.
- Rudnick, L., Katz-Stone, D. M., Anderson, M. C., 1994. *Astrophys. J. Sup. S.* 90, 955.
- Schneid, E. J., et al., 1992. *Astron. & Astrophys.* 255, L13.
- Sreekumar, P., et al., 1998. *Astrophys. J.* 494, 523.
- Stecker, F. W., 2005. *Phys. Rev. D* 72 (10), 107301.
- Stecker, F. W., Baring, M. G., Summerlin, E. J., 2007. *ArXiv:astro-ph/0707.4676* 707.
- The High Resolution Fly’s Eye Collaboration, 2002. *ArXiv:astro-ph/0208301*.

- The Pierre Auger Collaboration, 2007. *Science Journal* 318, 939.
- van Putten, M. H. P. M., 2005. *Gravitational Radiation, Luminous Black Holes and Gamma-Ray Burst Supernovae*. Cambridge University Press.
- Vietri, M., 1995. *Astrophys. J.* 453, 883.
- Vietri, M., De Marco, D., Guetta, D., 2003. *Astrophys. J.* 592, 378.
- Waxman, E., 2000. *Astrophys. J. Sup. S.* 127, 519.
- Waxman, E., Bahcall, J. N., 1997. *Phys. Rev. Let.* 78, 2292.
- Waxman, E., Bahcall, J. N., 1999. *Phys. Rev. D* 59, 23002.
- Yamamoto, T., et al., 2007. In: 30th International Cosmic Ray Conference. Vol. 7. p. 387.
- Yoshida, S., et al., 1995. *Astropart. Physics* 3, 105.